Tellus (1998), 50A, 545–556
Printed in UK – all rights reserved

TELLUS
ISSN 0280–6495

Salinity variability in the German Bight in relation to climate variability

By HAUKE HEYEN[1,*] and JOACHIM W. DIPPNER[2], [1]*GKSS Institute for Hydrophysics, Max-Planck Straße, D-21502 Geesthacht, Germany, and* [2]*Max-Planck Institute for Meteorology, Bundesstraße 55, D-20146 Hamburg, Germany*

(Manuscript received 17 November 1997; in final form 30 April 1998)

ABSTRACT

A relationship between observed variability in large-scale climate and salinity in the German Bight is sought using a multivariate statistical approach. It is found that on an annual timescale, 90% of the observed salinity variability is in-phase and correlated with a lag of several months to large-scale air pressure. The statistical model is used to estimate annual salinity anomalies from large-scale air pressure back to 1900. The correlations between estimated and observed salinities range from $r = 0.4$ to $r = 0.7$, depending on the position. It is shown that advective precipitation is the mechanism that links air pressure and salinity anomalies. Advection of Atlantic Water has only a minor impact on the annula mean in the examined coastal zone. If air pressure data from a climate change experiment is used as predictor, a slight drop of the mean salinity level in the range of 0.2 to 0.3 psu is predicted for the near future.

1. Introduction

The goal of this paper is to seek a link between salinity in the German Bight and the large-scale atmospheric circulation. If such a link can be found, it becomes possible (i) to reconstruct historical salinities and (ii) to estimate the impact of climate change on salinity. The reason is that the large-scale features of the atmospheric circulation are (i) well known back to 1900 (while local data is often gappy or does not exist), and (ii) realistically reproduced by General Circulation Models (GCMs). One reason for the interest in salinity is that anomalies in salinity are supposed to coincide with observed changes in the ecosystem, e.g., in species abundance and composition (Nehring, 1994; Lindeboom et al., 1995).

Hydrographical studies by Schott (1966) and Dickson (1971) revealed a connection between salinity variations in the North Sea and the atmospheric circulation, though both authors disagreed on the mechanism. While Schott (1966) found evidence that the surface salinities in the entire North Sea are dominated by large-scale atmospheric advection via precipitation, Dickson (1971) believes that advection of haline Atlantic Waters is the main cause.

Despite the fact that the German Bight is a coastal region with several estuaries, salinities > 34.8 psu are observed occasionally, clearly indicating an inflow of Atlantic Water through the English Channel (Kalle, 1937; Deutsches Hydrographisches Institut, 1984; Becker et al., 1992; Becker and Dooley, 1995). Atlantic Water entering the North Sea from the north mainly recirculates in the Dooley Current or north of the Doggerbank (Svendsen et al., 1995) and therefore does not influence the German Bight. In addition, the colonization of Atlantic zooplankton in the German Bight was observed after strong inflows through the Channel (Nehring, 1994) with significant impact on the local fauna (Zeiss and Kröncke, 1997; Kröncke et al., 1998).

* Corresponding author.

2. Data

2.1. Salinity data

Monthly mean surface values from 9 light vessels and the island of Helgoland are used (data from the Federal Maritime and Hydrographic Agency, Hamburg, FRG, hereafter BSH). The positions are shown in Fig. 1. Salinity was measured with interruptions between 1908 and 1995. During this period, most light vessels were relocated several times, leading to inconsistencies in the records. A homogenization is difficult, since the relocations were often only a few months apart, making it impossible to check whether they led to changes in the observed mean or standard deviation.

To find a statistical relationship between climate and salinity, only the light vessels LV Borkumriff, LV Weser, LV Elbe1 and LV P11/P8 were used. The first three were selected because they possess the longest observational records, the latter was included to obtain a more regular spatial distribution of stations. The records of these 4 vessels contain the following obvious inhomogeneities.

(a) Pre-war salinity observations at LV Borkumriff are about 0.5 psu (which corresponds to ≈ 1 standard deviation σ that station) higher than post-war observations. The reason is the relocation in March 1954, 20 km eastward from its pre-war position.

(b) In 1972 the observed mean salinity at LV P11/P8 increases by about 0.9 psu ($\approx 1.2\sigma$) while the σ decreases by about 25%. Simultaneously LV P11/P8 was moved 50km westward.

(c) At LV Elbe1 the observed pre-war salinity mean is about 0.5 psu ($\approx 0.5\sigma$) lower than the post-war one. LV Elbe1 was withdawn in August 1939 and reestablished in August 1945 3km southwest from its pre-war position. Relocations within the same distance took place 7 times between 1924 and 1988, but the discrepancy between pre- and post-war salinity levels is the only obvious inhomogeneity in the time series of LV Elbe1.

For the following calculations, the inhomogeneities at LV Borkumriff and LV P11/P8 were roughly corrected by setting them to a constant mean and σ. The reason for the inhomogeneity at LV Elbe1 is unknown, therefore no correction was applied.

2.2. Other data

Sea level air pressure on a $5^\circ \times 5^\circ$ grid (analysis data from the National Center for Atmospheric Research, Boulder, USA, hereafter NCAR; Trenberth and Paolino, 1980) are used as large-scale predictor. The selected box covers 70°W to 15°E and 30°N to 70°N.

The climate scenario data comes from the global coupled ocean-atmosphere ECHAM3/LSG model* with T21 resolution ($\approx 5.6^\circ \times 5.6^\circ$, data from the Deutsches Klimarechenzentrum, Hamburg, FRG, hereafter DKRZ; Cubasch et al., 1995). The chosen experiment starts in 1880 and is forced with observed greenhouse-gas and aerosol concentrations until 1985; afterwards the 'business as usual' scenario from the Intergovernmental Panel on Climate Change (IPCC) is assumed until 2049. This scenario considers a yearly increase of CO_2 by 1.3% and estimated future aerosol concentrations (Hasselmann et al., 1995).

To understand the physical mechanisms that link large-scale air pressure and salinity, the following datasets are used:

- Monthly means of precipitation (data from NCAR). 7 stations with less than 100 missing values between 1924 and 1988 were selected (Fig. 1).
- Monthly means of river transports (data from the Global Runoff Data Centre, Koblenz, FRG, hereafter GRDC). 5 stations were selected that measured between 1924 and 1988 without longer interruptions (Fig. 1).
- The North Atlantic Oscillation (NAO) Index (Hurrell, 1995). This yearly index gives the difference between the air pressure at Lisbon and Stykkisholmur (Iceland) in winter. A high index is generally associated with westerly winds and mild winters in Europe.
- Daily air pressure (data from NCAR) was used to estimate wind stress on the sea surface via an empirical bulk formula (Duun-Christensen, 1975).
- The variance of air pressure (data from NCAR) on the 2.5 to 6 days frequency band was calculated as a proxy for storm activity (Blackmon, 1976).

* European Center HAMburg/Large Scale Geostrophic.

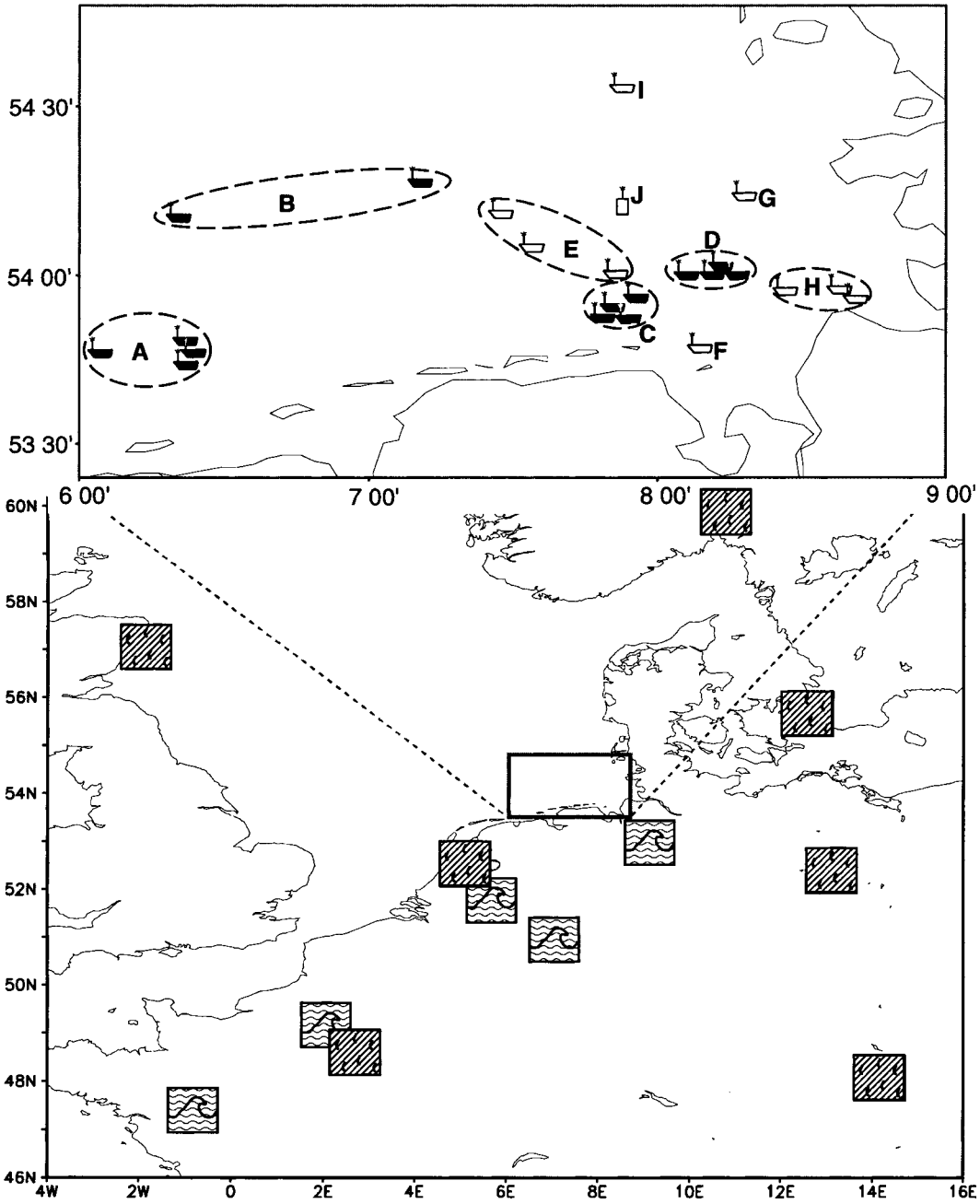

Fig. 1. Salinity (top). Black vessels were used for the establishing of the model, white vessels for additional validation. Dashed circles indicate the range within which relocations took place. A: LV Borkumriff, B: LV P11/P8, C: LV Weser, D: LV Elbe1, E: LV P15/P12, F: LV Bremen, G: LV Ausseneider, H: LV Elbe4, I: LV Amrumbank, J: Helgoland Roads. *Precipitation* (rain drop symbol): Aberdeen, Paris, De Bilt, Oslo, Kopenhagen, Potsdam, Kremsmünster (from west to east). *River transports* (wave symbol): Montjean (Loire), Paris (Seine), Lith (Maas), Köln (Rhein) and Intschede (Weser) (from west to east).

3. Method

The steps of the applied method are as follows:

(1) A relationship is sought between the anomalies of air pressure and salinity by fitting a statistical model for different combinations of timescales and time lags. For the fit, data from 4 light vessels and the period 1955 to 1974 is used. Data from the years 1924 to 1954 and 1975 to 1988 are used for validation.

(2) The combination with the best skills in the fit and the validation period is selected.

(3) The selected model is validated with data from 6 additional stations.

(4) To find the physical explanation for the identified relationship, associated patterns of wind, precipitation, etc. are calculated.

(5) Large-scale pressure data from a General Circulation Model (GCM) climate change experiment is used as input for the statistical model. The resulting salinity estimates are compared to historical observations with respect to changes in mean and variability.

Details about these steps are given in the following subsections.

3.1. *Searching for a relationship*

A relationship between air pressure and salinity was sought, using 1-, 3-, 6-, 9-, 12- and 15-monthly averages of (i) air pressure at the 18×9 grid points (see above) and (ii) salinity at the 4 light vessels LV Borkumriff, LV P11/P8, LV Weser and LV Elbe1. Since the interannual variability is to be examined, the seasonal cycle was subtracted. For each specific combination of seasons, a different statistical model was built, since it is not certain whether climatic influence on salinity is constant throughout the year (for example, one model was built between January air pressure and December to February salinity, another model between February air pressure and December to February salinity). A possible delay of up to 24 months between the signal in air pressure and the impact on salinity was taken into account.

3.2. *The statistical model*

The statistical model follows the idea of "statistical downscaling" by von Storch et al. (1993). For each tested combination of mean, season and time lag, the model is built as follows: Firstly, Empirical Orthogonal Functions (EOFs, also called Principal Components) of air pressure and salinity anomalies are calculated. Secondly, a Canonical Correlation Analysis (CCA) is performed between the leading EOFs of both parameters. For details on EOFs and CCA see Preisendorfer (1988) or von Storch (1995).

The characteristic of EOFs is that their leading eigenmodes (also called "patterns" and "time series") represent the major part of the variance of the depicted parameter. For example, the dominating atmospheric mode in the selected air pressure box is the NAO, which accounts for ca. 40% of air pressure variance in the monthly mean. Therefore, the 1st EOF-pattern of air pressure describes the spatial structure of the NAO, i.e., low air pressure at the northern stations and high air pressure at the southern stations (or vice versa). The 1st EOF-time series modulates this pattern.

Only the leading eigenmodes of air pressure and salinity are used in this study for the following reasons: Firstly, historical climate data will be used to reconstruct the salinity record. While historical data might be gappy or inhomogeneous at single stations, its spatial structure can be estimated more reliably using data from many stations. Secondly, GCM scenario data will be used. Though GCMs are capable of reproducing the main features of the atmospheric fields, their information on single gridpoints is unreliable (Robinson and Finkelstein, 1991). Thirdly, it is certainly not possible to reconstruct every salinity variation at each station in detail, but it might be possible to reconstruct the main features of the variability in that area. Fourthly, the truncation of trailing eigenmodes keeps the degrees of freedom of the model low, minimizing the danger of high correlations due to overfitting.

For air pressure, the eigenmodes were calculated from the covariance matrix, therefore atmospheric structures with high variance dominate the leading eigenmodes. We expect that such structures, e.g., the NAO, will cause the largest effects on the local climate. Four EOFs are used, which represent 80% to 90% of monthly air pressure variability. The eigenmodes of salinity were calculated from the correlation matrix, to account for the differences in variance between the light vessels. Only the 1st EOF was used, that represents more than 90% of monthly salinity anomalies.

The CCA identifies a linear combination of air pressure-eigenmodes and a linear combination of salinity-eigenmodes that are maximum correlated with each other. This property allows to search for relationships, even if it is not known for which timescale, season and time lag they might exist.

3.3. Regression

Let $G(x, t)$ and $L(x, t)$ be the observed anomalies of air pressure and salinity in the fitting period at station x and time t. Assume that the leading eigenmodes of $G(x, t)$ and $L(x, t)$ are already known. The CCA identifies i patterns Γ_i, Λ_i and i normalized time series γ_i, λ_i, which are linear combinations of the eigenmodes of $G(x, t)$ and $L(x, t)$. ρ_i is the correlation between the ith pair of time series. Let $G'(x, t)$ be air pressure data from the independent period. The goal is to estimate salinity $\hat{L}(x, t)$ for this period from $G'(x, t)$. This is done as follows:

(1) Assume that $G(x, t)$ and $G'(x, t)$ share the same Γ. Projecting $G'(x, t)$ onto Γ, the Euclidean distance

$$\left\| G'(x, t) - \sum_{i=1}^{I} [\Gamma_i(x) \times \gamma_i'(t)] \right\|$$

is minimized to calculate the new time series γ'.

(2) Assuming that γ_i' is correlated to a time series λ_i' in the same manner as γ_i and λ_i were, λ_i' is estimated as $\lambda_i' = \rho_i \times \gamma_i'$.

(3) If $\hat{L}(x, t)$ and $L(x, t)$ share the same Λ, the best guess is

$$\hat{L}(x, t) = \sum_{i=1}^{I} [\Lambda_i(x) \times \lambda_i'(t)] .$$

The same method was used by Heyen et al. (1996).

3.4. Selection of one specific combination

Three criteria are used to select one specific combination of mean, season and time lag. Firstly, a high correlation r during the fitting period is needed to indicate a possible relationship. Secondly, a high correlation r during the validation period should exist, indicating that the relationship is stable. Finally, the error of the model β should be small, to ensure the model is useful for reconstructions or predictions. β is also known as the "Brier-based score against the relative climatology" (Livezey, 1995): $\beta = 1 - \mathrm{Var}[t_{\mathrm{obs}} - t_{\mathrm{mod}}]/\mathrm{Var}[t_{\mathrm{obs}}]$, with t_{obs} and t_{mod} being the observed and modeled time series, and $\mathrm{Var}[z]$ being the variance of z. $\beta = 1$ means that model and observation are identical, $\beta = 0$ that the error of the model has the same size as the variance of the observations.

In the following, we will refer to the correlation coefficent r and the model error β as the "skill factors" or "skill of the model".

3.5. Associated patterns

If it is suspected that the relationship between predictor and predictand is indirect, associated patterns (Heyen et al., 1996) may help to identify the missing link. The missing link should be highly correlated with the identified CCA-time series λ (or γ). Therefore, a potential link $\boldsymbol{D}$ is tested by minimizing the Euclidean distance

$$\left\| D(y, t) - \sum_{i=1}^{I} [\Delta_i(y) \times \lambda_i(t)] \right\| ,$$

where $D(y, t)$ are the observations of the tested variable at station y and time t, and Δ_i is the sought associated pattern of $\boldsymbol{D}$ with respect to λ_i. If $D(y, t)$ is the sought link, Δ_i should explain a high amount of variance. "Explained variance" is defined analogously to β: For example, assuming that Δ consists of n stations y, the explained variance $v(y)$ at station y computed as

$$v(y) = \left(1 - \frac{\mathrm{Var}[D(y, t) - \Delta(y) \times \lambda(t)]}{\mathrm{Var}[D(y, t)]} \right) \times 100 .$$

The "explained variance of the pattern Δ'' is then $\bar{v} = n^{-1} \Sigma_{y=1}^{n} v(y)$. A practical application is given in Subsection 4.2.

4. Results

4.1. An optimized statistical relationship

The statistical model was built with 4 air pressure EOFs and 1 salinity EOF. These explain 80% to 95% of air pressure and salinity variance for all tested averages and seasons. The structure of the obtained results can be seen in Fig. 2. A high model skill is found for averages of approximately one year or longer. A salinity mean centered around the summer months is correlated to an air pressure mean about 6 to 18 months earlier.

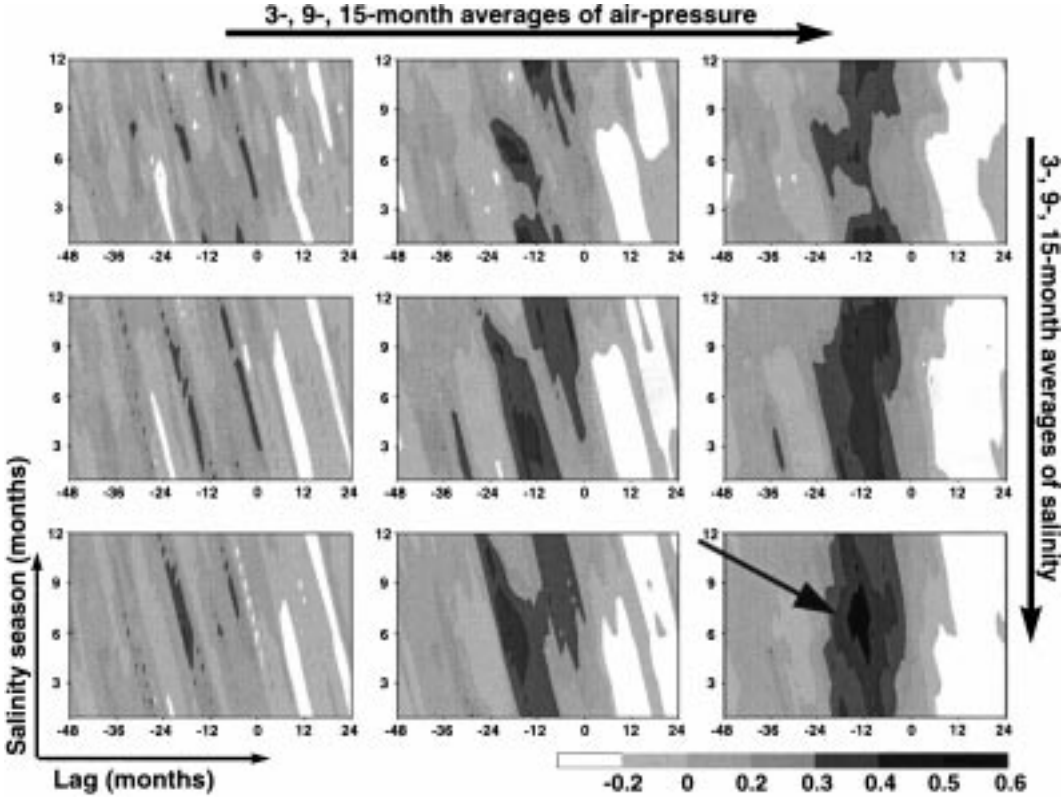

Fig. 2. Skill r of the model for different combinations of averages (top to bottom: 3-, 9- and 15-month averages of salinity; left to right: 3-, 9- and 15-month averages of SLP), salinity season (y-axis) and time lag (x-axis, negative values mean that SLP is leading). High correlations are found for long averages. The highest correlation (arrow) exists between a 15-month average of salinity, centered around the summer months, and a 15-month average of SLP, approximately 12 months earlier.

Within this range, the skill of the model is relatively unsensitive against the chosen season and time lag, probably due to the long averages that are used.

The criteria for the selection of one specific result are (i) a high skill and (ii) as short averages as possible, in order to identify the time lag and the underlying processes more precisely.

We selected a 12-month average of salinity, centered around August, and a 9-month average of air pressure, centered around the previous November. The features of this relationship are as follows:

The 4 leading eigenmodes of air pressure explain 88% of variability. The 1st leading eigenmode of salinity explains 94% of variability and has a uniform sign. This means that 94% of all variability in the annual mean occur in-phase at all 4 light vessels.

The CCA-patterns (Fig. 3) show a positive pressure anomaly of typically 2 hPa over Europe that is correlated with a positive salinity anomaliy of typically 0.5 psu in the German Bight. Table 1 depicts the skill of the model at the 4 stations for the fitting and the validation period. The differences in obtained skill will be adressed in the discussion section.

Fig. 4 shows the observed and estimated salinity time series. The model reproduces the interannual variability fairly well. The correlation between estimated salinity and observation data from other stations (Fig. 5, Table 1) indicates that the major part of the variability is in-phase across the entire

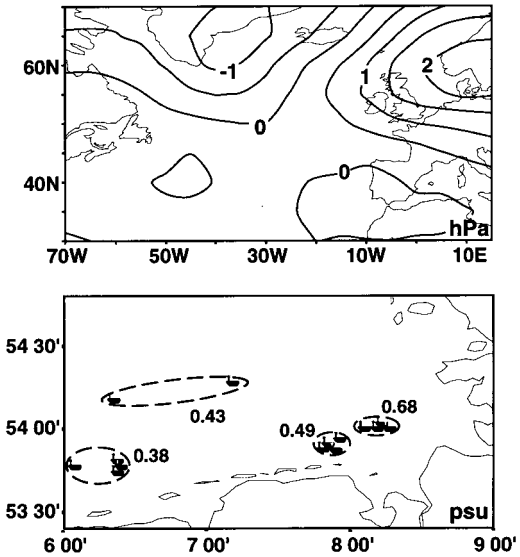

Fig. 3. 1st pair of CCA-patterns between July to March air pressure anomalies (top) and of following March to February salinity anomalies (bottom). A positive pressure anomaly of typically 2 hPa above northern Europe occurs together with positive salinity anomalies of typically 0.5 psu in the German Bight. The time series of both patterns are correlated with $r = 0.7$ within the fitting period.

German Bight and, hence, that the estimated time series is valid for the entire region.

4.2. Physical mechanism

To determine the causes for the statistical relationship between air pressure and salinity, the associated patterns of storm activity, wind stress, precipitation and the NAO-index are calculated with respect to the time series of the SLP CCA-pattern from Fig. 3.

The associated pattern of storm activity explains only 10% of variance over Europe and the North Atlantic. This means that the overwhelming portion of storm activity is not correlated to the occurrence of the CCA air pressure pattern from Fig. 3. The correlation between NAO-index and the time coefficients of the CCA air pressure pattern is $r = 0.2$. It can be concluded that neither variability in storm activity, nor variability in the NAO can explain the found relationship between air pressure and salinity. The associated pattern for the west-east component of the wind stress explains 50% of variance over the English Channel, a westerly wind stress coincides with low salinities. The associated pattern for the north-south component explains 70% of variance over the northern North Sea, a northerly wind stress coincides with low salinities. This result is not shown, since it follows from the air pressure pattern in Fig. 3.

The associated pattern of precipitation shows that 72% (De Bilt), 61% (Potsdam, Kopenhagen), 32% (Oslo), 30% (Paris), 24% (Aberdeen) and 9% (Kremsmünster) of precipitation variance are associated with the air pressure pattern in Fig. 3. The depicted anticyclone over northern Europe coincides with low precipitation and high salinities.

It is concluded that the anticyclonic air pressure

Table 1. *r and β of the model for the fitting period (left columns), the validation period (middle columns), and the entire period (right columns; the r and β are given for 1- and 2-year running averages); numbers in brackets indicate the number of available years; in case of the 6 lower stations β was optimized by multiplying the modeled salinity with a constant*

	Fit. period 1955–1974	Val. period 24–54, 75–88	1-yr, 2-yr averages 1924–1988
LV Borkumriff	0.65/0.42 (20)	0.60/0.34 (32)	0.63/0.39, 0.76/0.54 (52)
LV P11/P8	0.75/0.53 (20)	0.47/−0.86 (10)	0.61/0.24, 0.71/0.22 (30)
LV Weser	0.53/0.24 (20)	0.46/0.06 (30)	0.51/0.22, 0.63/0.31 (50)
LV Elbe1	0.63/0.38 (20)	0.26/−0.26 (37)	0.41/0.16, 0.40/0.13 (57)
LV P15/P12	—	—	0.60/0.32, 0.58/0.27 (33)
LV Bremen	—	—	0.62/0.33, 0.67/0.33 (21)
LV Ausseneider	—	—	0.54/0.16, 0.60/0.05 (17)
LV Elbe4	—	—	0.53/0.22, 0.61/0.26 (20)
LV Amrumbank	—	—	0.50/0.21, 0.56/0.26 (17)
Helgoland Roads	—	—	0.52/0.24, 0.57/0.28 (66)

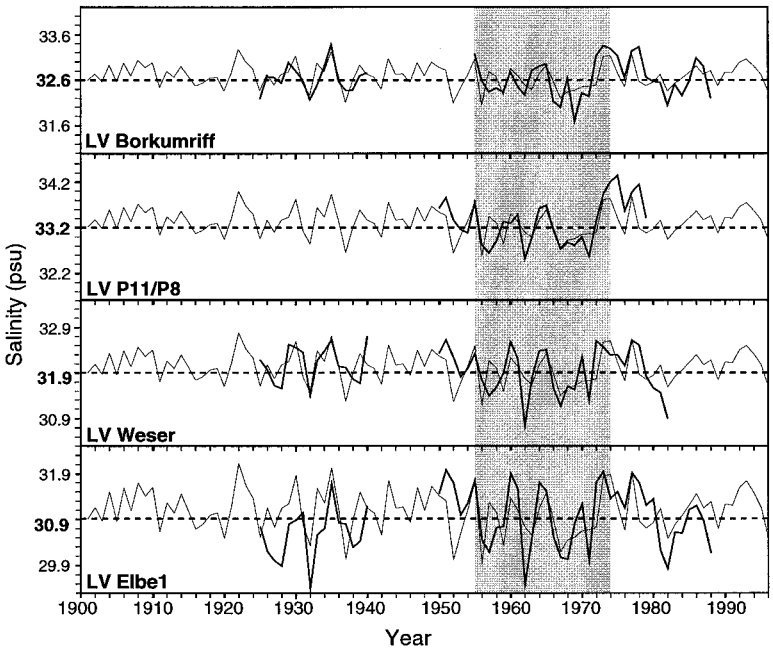

Fig. 4. Estimated (thin) and observed (thick) annual salinity. The hatched area indicates the fitting period of the model.

pattern from Fig. 3 leads to easterly winds over western Europe that hinder a large-scale advection of marine air to Europe and cause reduced precipitation (or vice versa). This connection is strongest in the southern North Sea region. Reduced precipitation leads to higher salinity levels (or vice versa). The time lag between the occurrence of the air pressure pattern and changes in the salinity leads to the conclusion that the impact of precipitation is indirect, i.e., via runoff.

This hypothesis can be proved when 12-month averages of river transport are correlated with the salinity observations. The closer the river estuaries are situated to the German Bight, the higher the correlation and the shorter the lag (Fig. 6).

4.3. Climate change scenario

The model is capable of reconstructing interannual variability, therefore it makes sense to run it with air pressure data from a climate change experiment in order to determine whether systematic changes will occur. Comparing Fig. 7 with Fig. 4 it can be seen that the estimated salinity time series has a smaller variance than do the observations. Also, the mean salinity drops slightly after the model year 2000.

A comparision between observed and estimated mean and variability for different periods is given in Table 2. The loss of variance is an artefact of our model, since it occurs in the estimations from historical data and GCM data. The drop in the mean after the year 2000 is due to a signal in the GCM data. Analysis of different GCMs by the IPCC showed that these models predict an increase of precipitation in high latitudes in winter (Houghton et al., 1996). Thus, the results of the statistical model are consistent with these results.

5. Discussion

Three points are addressed in this discussion: the differences in skill for the different light vessels and the reasonableness of the found time lag. Finally, the presented results will be compared with the results of Schott (1966) and Dickson (1971).

Diffferences in skill (between $r = 0.7$ and $r = 0.4$, depending on the station) show that local

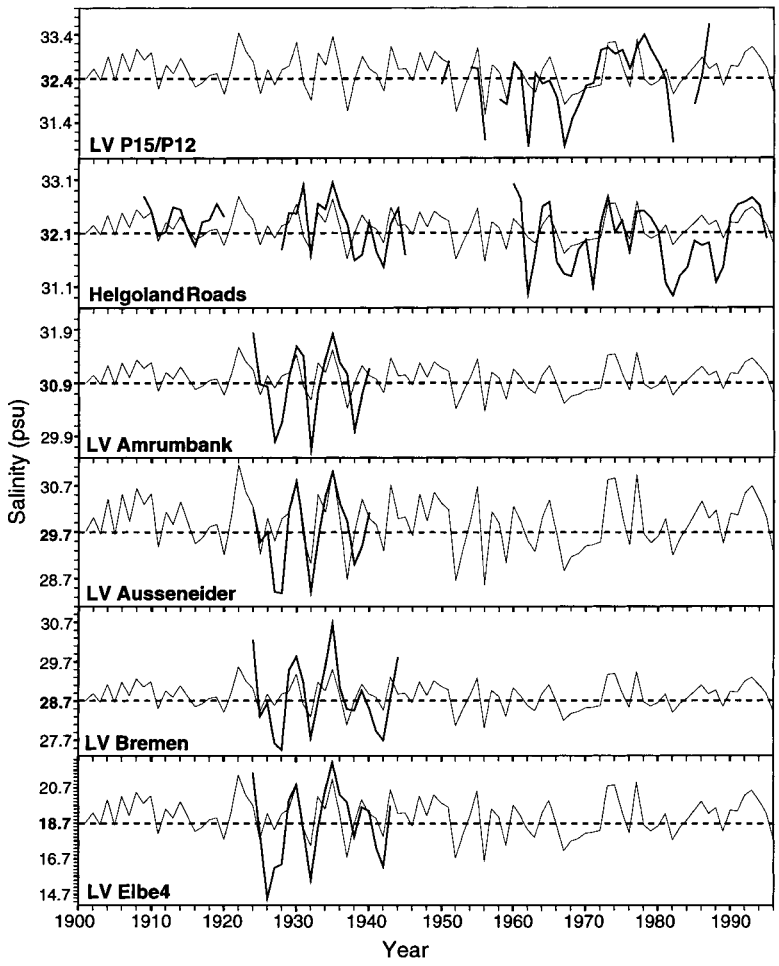

Fig. 5. Estimated (thin) and observed (thick) annual salinity. The scale of the *y*-axis varies.

salinity variations exist beside the simultaneous rise and fall. We think that local orography and dynamics lead to these differences: Some of the stations, e.g., LV Borkumriff, are situated in a well-mixed water mass, hence, advection by winds and tides or even modest relocations do not disturb the measurements much. Other stations, such as LV Elbe1, are situated within the inner German Bight where mesoscale eddies and frontal systems with high horizontal gradients up to 0.4 psu/km occur (Dippner, 1992 and 1995). LV Elbe4 is situated in an estuary with no mesoscale eddies, but high gradients. High gradients cause a high variability in the measurements if the water body is moved by winds and tides. In addition, any relocation causes inhomogeneities. Hence, salinity records from different stations contain different processes and possess a different degree of homogeneity.

The length of the found time lag leads to the conclusion that precipitation effects the salinity indirectly via river discharge. Fig. 6 shows that a signal in the transport needs several months to reach the German Bight. This is reasonable, since in the near-coastal zone the signal travels with the speed of the tidal residual current, which is typically 1 cm/s to 2 cm/s (Maier-Reimer, 1977) and several 100km lie between the river estuaries and

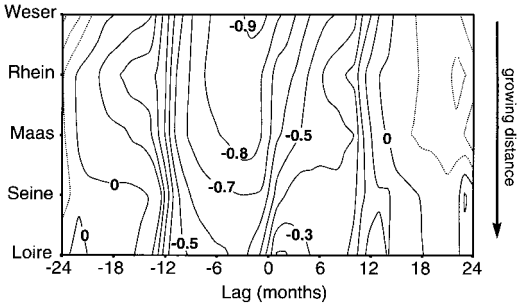

Fig. 6. Correlation r between annual means of observed transport and salinity in dependence from the distance between estuary and German Bight (y-axis) and time lag (x-axis, negative values mean that river transport is leading). The shorter the distance, the higher the correlation and the shorter the lag.

the German Bight. Another factor of delay may be that winter storage as snow delays the runoff of precipitation into the rivers.

It should be noted, too, that the found lag is only a rough estimation. The signal in Fig. 2 is fuzzy and high skills can be obtained for a couple of neighbouring combinations. The reason is probably that the precipitation signal reaches the German Bight with different delays, depending on the traveled distances. The different delays explain, too, why an annual average was necessary to detect the signal.

Schott (1966) estimated the quantities of Atlantic advection, freshwater advection, precipitation and evaporation for different regions in the North Sea. In addition, he cross-correlated salinity anomalies in different regions with each other and with river runoff, precipitation and the west wind

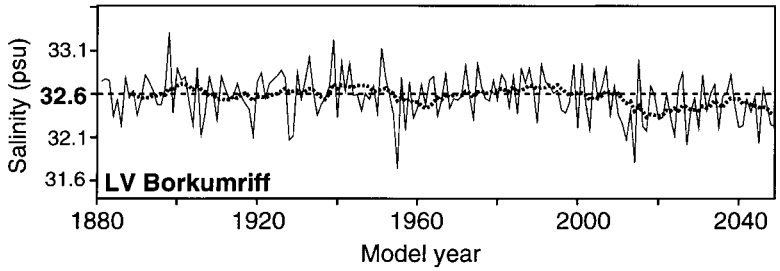

Fig. 7. Estimation of annual mean salinity anomalies (against the mean of the fitting period) at LV Borkumriff for the climate change scenario "business as usual". The thick line represents the 10-year running mean. The given years are model years and cannot be transferred to calendar years.

Table 2. *Mean and standard deviation (upper and lower value) of the observed and estimated salinity anomaly*

	Observed 1924–1988	Model 1924–1988	Model (GCM) 1880–1930	Model (GCM) 1939–1989	Model (GCM) 1999–2049
LV	0.04	0.07	0.00	0.02	−0.14
Borkumriff	0.38	0.26	0.25	0.25	0.27
LV	0.13	0.08	0.00	0.02	−0.16
P11/P8	0.50	0.29	0.28	0.29	0.31
LV	0.09	0.10	0.00	0.02	−0.18
Weser	0.48	0.33	0.32	0.32	0.35
LV	−0.02	0.13	0.00	0.03	−0.25
Elbe1	0.66	0.46	0.44	0.45	0.49

The reference level for the salinity anomalies is the fitting period; the negative mean at LV Elbe1 during the observation period is the result of the discussed inhomogeneity. The change in sign for the mean salinity after the model year 2000 is obvious.

component. He found correlations between river runoff and long-term salinity anomalies across the entire North Sea. This led him to the conclusion that the observed anomalies in the surface salinity are driven primarily by large-scale precipitation that are induced by anomalies in the west wind component. Dickson (1971) presented a specific atmospheric circulation pattern with a trough centered over the North Atlantic and a ridge over western Europe that occurred together with increased salinity levels in the North Sea. He argues that this pattern causes the advection of more (or more haline) Atlantic Water to the North Sea. Since he found an increased lag for salinity anomalies from the English Channel to the German Bight, he concluded that oceanic advection dominates the long-term salinity anomalies in the entire North Sea.

The air pressure CCA-pattern identified in this study (Fig. 3) is different to the the pattern of Dickson (1971). One difference is the position of the isobars above the English Channel. While in Dicksons' pattern anticyclonic activity above western Europe favours a geostrophic transport through the Channel into the North Sea, anitcyclonic activity in Fig. 3 will rather block an inflow — as the associated patterns revealed, more than 50% of variance of westerly wind stress over the English Channel and northerly wind stress over the northern North Sea are associated with lower salinities, contradicting the theory of advection. This difference between Fig. 3 and Dicksons' pattern may be partly explained by the fact that Dickson used a preclassified pattern (Namias, 1964 and 1965), while the CCA-pattern is optimized. Partly it may be due to the fact that Dickson used charts of the 500 mbar and 700 mbar level and had to guess the surface displacements of the troughs and ridges, since no surface charts were available at his time.

To conclude, the identified CCA-pattern rather supports Schotts' theory of increased western advection. Also, the increasing lag in the correlations between salinity anomalies and river discharges (Fig. 6) shows that freshwater impact on salinity is strong, what supports Schott, too. However, since the presented model was optimized for stations that lie mainly between the coast and the tidal mixing front, it allows no general conclusions about other regions in the North Sea.

6. Acknowledgements

The authors are indebted to Hans von Storch and Eduardo Zorita for the fruitful discussions shedding light on new aspects on the above subject. Thanks to E. Schamidatus (BSH), Dr. W. Grabs (GRDC) and Dr. J. Hurrel (NCAR) for their unbureaucratic provision of data. Finally, many thanks to the unknown crews who took the samples under all weather conditions. The project was funded by the European Community under DYNAMO, FAIR-CT95-0710.

REFERENCES

Becker, G. A., Dick, S. and Dippner, J. W. 1992. Hydrography of the German Bight. *Mar. Ecol. Prog. Ser.* **91**, 9–18.

Becker, G. A. and Dooley, H. D. 1995. The 1989/91 high salinity anomaly in the North Sea and adjacent areas. *Ocean Challenge* **6**, 52–57.

Blackmon, M. L. 1976. A climatological spectral study of the 500 mbar geopotential height of the northern hemisphere. *J. Atmos. Science* **33**, 1607–1623.

Cubasch, U., Hegerl, G., Hellbach, A., Höck, H., Mikolajewicz, U., Santer, B. D. and Voss, R. 1995. A climate change simulation starting from 1935. *Clim. Dyn.* **11**, 71–84.

Deutsches Hydrographisches Institut 1984. Deutsche Bucht, Hydrographie. *Meereskundliche Beobachtungen und Ergebnisse* **57**, 166 p.

Dickson, R. R. 1971. A recurrent and persistent pressure-anomaly pattern as the principle cause of intermediate-scale hydrographic variation in the european shelf-seas. *Dt. Hydrogr. Zt.* **24**, 97–119.

Dippner, J. W. 1992. Mesoscale variability of the German Bight — an atlas of circulation, density distribution and sea surface height. *Institut für Meereskunde Technical Report* **2**, 87 p.

Dippner, J. W. 1995. Untersuchung transienter Wirbelstrukturen in der Deutschen Bucht. *Berichte aus dem Zentrum für Meeres- und Klimaforschung* **B18,** 146 p.

Duun-Christensen, J. T. 1975. The presentation of the surface air pressure field in a two dimensional hydrodynamic model for the North Sea, the Skagerrak and the Kattegatt. *Dt. Hydrogr. Zt.* **28**, 97–116.

Hasselmann K., Bengtsson, L., Cubasch, U., Hegerl, G. C., Rodhe, H., Roeckner, E., von Storch, H., Voss, R. and Waszkewitz, J. 1995. Detection of anthropogenic

climate change using a fingerprint method. In: *Proceedings "Modern Dynamical Meteorology", Symposium in Honour of Aksel Wiin-Nielsen*, Ditlevsen, P. (ed.). ECMWF press, pp. 203–221.

Heyen, H., Zorita, E. and von Storch, H. 1996. Statistical downscaling of monthly mean North Atlantic air pressure to sea level anomalies in the Baltic Sea. *Tellus* **48A**, 312–323.

Houghton, J. T., Meira Filho, L. G., Callander, B. A., Harris, N., Kattenberg, A. and Maskell, K. (eds.) 1996. *Climate change 1995. The science of climate change*. Contribution of working group I to the 2nd assessment report of the IPCC. University Press, Cambridge, pp. 42–45.

Hurrell, J. W. 1995. Decadal trends in the North Atlantic Oscillation: regional temperatures and precipitation. *Science* **269**, 676–679.

Kalle, K. 1937. Nährstoff-Untersuchungen als hydrographisches Hilfsmittel zur Unterscheidung von Wasserkörpern. *Annalen der Hydrographie und Maritimen Meteorologie* **65**, 1–18.

Kröncke, I, Dippner, J. W., Heyen, H. and Zeiss, B. 1998. Long-term changes in macrofauna communities off Norderney (East Frisia, Germany) in relation to climate variability. *Mar. Ecol. Progr. Ser*., in press.

Lindeboom, H., van Raaphorst, W., Beukema, J., Cade}-bae, G. and Swennen, C. 1995. (Sudden) changes in the North Sea and Wadden Sea: Oceanic influences underestimated? *Dt. Hydrogr. Zt*. (suppl. 2), 87–100.

Livezey, R. E. 1995. The evaluation of forecasts. In: *Analysis of climate variability*, von Storch, H. and Navarra, A. (eds.). Springer Verlag, pp. 177–196.

Maier-Reimer, E. 1977. Residual circulation in the North Sea due to the M_2-tide and mean annual wind-stress. *Dt. Hydrogr. Zt*. **30**, 69–80.

Namias, J. 1964. Seasonal persistence and recurrence of European blocking during 1958–60. *Tellus* **30**, 394–407.

Namias, J. 1965. Short period climatic fluctutation. *Science* **147**, 696–706.

Nehring, S. 1994. Gymnodinium catenatum Graham (Dinophyceae) in Europe: A growing problem? *J. Plankton Res.* **17**, 85–102.

Preisendorfer, R. W. 1988. *Principal component analysis in meteorology and oceanography*, Mobley, C. D. (ed.). Elsevier Science Publishers, Amsterdam.

Robinson, P. J. and Finkelstein, P. L. 1991. The development of impact-oriented scenarios. *Bull. Amer. Met. Soc*. **4**, 481–490.

Schott, F. 1966. Der Oberflächensalzgehalt in der Nordsee. *Dt. Hydrogr. Zt*. (suppl. A9), pp. 1–58.

Svendsen, E., Aglen, A., Iversen, S. A., Skagen, D. W. and Smedstadt, O. 1995. Influence of climate on recruitment and migration of fish stocks in the North Sea. In: "Climate change and northern fish population", by Beamish, R. J. (ed.). *Can. J. Fish. Aquat. Sci.* **121**, 641–653.

Trenberth, K. E. and Paolino, Jr., D. A. 1980. The northern hemisphere SLP-dataset: trends, errors and discontinuities. *Mon. Wea. Rev*. **112**, 1999–2015.

von Storch, H., Zorita, E. and Cubasch, U. 1993. Downscaling of global climate change estimates to regional scales: An application to Iberian rainfall in wintertime. *J. Climate* **6**, 1161–1171.

von Storch, H. 1995. Spatial patterns: EOF and CCAs. In: *Analysis of climate variability*, von Storch, H. and Navarra, A. (eds.). Springer Verlag, pp. 227–253.

Zeiss, B. and Kröncke, I. 1997. Macrofauna long-term studies in a subtidal habitat off Norderney (East Frisia, Germany) from 1978 until 1994. *Oceanologica acta* **20**, 311–318.